Environ Monit Assess (2020) 192:457
https://doi.org/10.1007/s10661-020-08430-y

Interaction effects of the main drivers of global climate change on spatiotemporal dynamics of high altitude ecosystem behaviors: process-based modeling

Kadir Yildiz · Nusret Karakaya · Seref Kilic · Fatih Evrendilek

Received: 11 April 2020 / Accepted: 17 June 2020

Abstract Soil organic carbon and nitrogen (SOC-N) dynamics are indicative of the human-induced disturbances of the terrestrial ecosystems the quantification of which provides insights into interactions among drivers, pressures, states, impacts, and responses in a changing environment. In this study, a process-based model was developed to simulate the eight monthly outputs of net primary productivity (NPP), SOC-N pools, soil C:N ratio, soil respiration, total N emission, and sediment C-N transport effluxes for cropland, grassland, and forest on a hectare basis. The interaction effect of the climate change drivers of aridity, CO_2 fertilization, land-use and land-cover change, and best management practices was simulated on high altitude ecosystems from 2018 to 2070. The best management practices were developed into a spatiotemporally composite index based on SOC-N stock saturation, 4/1000 initiative, and RUCLE-C factor. Our model predictions differed from the remotely sensed data in the range of −64% (underestimation) for the cropland NPP to 142% (overestimation) for the grassland SOC pool as well as from the global mean values in the range of −97% for the sediment C and N effluxes to 60% for the total N emission from the grassland. The interaction exerted the greatest negative impact on the monthly sediment N efflux, total N emission, and soil respiration from forest by −90.5, −82.7, and −80.3% and the greatest positive impact on the monthly sediment C effluxes from cropland, grassland, and forest by 139.3, 137.1, and 133.3%, respectively, relative to the currently prevailing conditions.

Keywords Best management practices · Carbon and nitrogen cycles · Ecosystem biogeochemistry · STELLA model simulation

K. Yildiz · N. Karakaya · F. Evrendilek (✉)
Department of Environmental Engineering, Faculty of Engineering, Bolu Abant Izzet Baysal University, Bolu, Turkey
e-mail: fevrendilek@ibu.edu.tr

K. Yildiz
e-mail: kadiryildiz@ibu.edu.tr

N. Karakaya
e-mail: karakaya_n@ibu.edu.tr

S. Kilic
Department of Environmental Engineering, Faculty of Engineering, Ardahan University, Ardahan, Turkey
e-mail: serefkilic@ardahan.edu.tr

Published online: 27 June 2020

Introduction

Soil organic carbon and nitrogen (SOC-N) dynamics are stoichiometrically coupled to one another and biogeochemically link the (a)biotic components of a given terrestrial ecosystem. The spatiotemporal SOC-N dynamics are one of the most important indicators of ecosystem-level productivity and health (O'Rourke et al. 2015). The ecosystem structure (e.g., biodiversity and phenology) and function (e.g., energy flows and biochemical cycles) in higher altitudes are most sensitive to climate change since the biogeochemical cycles show distinct patterns in snow-covered and snow-free seasons (Elmendorf et al. 2012; Ernakovich et al. 2014).

Climate change, land-use and land-cover change (LULCC), and management practices are the main drivers of change, in particular, in the high altitude ecosystems, which act as the water tower and influence the water quality and quantity of the upper and lower watersheds.

Since the human-induced alterations of the C and N cycles are the main drivers of global climate change, numerous data-driven and process-based models of the C and N dynamics at the ecosystem level have been developed in related literature (Piao et al. 2020). However, how to sustainably manage the spatiotemporal dynamics of the ecosystem C and N stocks and fluxes depends on how to best take into account the interaction (multiplicative) effects. For example, Stehfest et al. (2019) used five integrated assessment models, the state-of-the-art global climate-energy-economy models, to assess the interaction among the six drivers of population, wealth, consumption preferences, agricultural productivity, land-use regulation, and trade. They reported that changes in population, agricultural efficiency, land-use regulation, and consumption behaviors most influenced the future expansion of cropland and pasture as well as most reduced food-security risks (Stehfest et al. 2019). Based on the four process-based ecosystem models of BIOME-BGC, JULES, ORCHIDEE, and O-CN, Churkina et al. (2010) found that the interaction among N deposition, LULCC, and climate change led to a mean C sequestration rate of 56 ± 39 Tg C year^{-1} by the European ecosystems between 1951 and 2000 due to the CO_2 and N fertilization effects on vegetation regrowth. From their meta-analysis, He et al. (2019) identified the interaction (nonadditive) effect of climate change and LULCC on biodiversity-related ecosystem services. To detect the effect of the interaction mechanism between climate change and LULCC on soil fauna, Yin et al. (2019) conducted an experimental field study by reconstructing two climatic and five land-use regimes. Peters et al. (2019) pointed out that ecosystem function was more severely altered in the arid lowlands and the cold highlands due to the interaction between the drivers of climate and land use instead of the individual main (additive) effects of the drivers. Xiong et al. (2014) stated that the SOC sequestration rate was the product of climate factors and ecosystem type.

There still exists a large knowledge gap about how to quantify and input the interaction among climate change, LULCC, and management practices into the decision-support systems. Relying only on the main effects of econometric, ecological, or technological drivers instead of their interaction effects does not portray a realistic understanding of how to best take into account the sustainable development strategies during the process of decision-making. Therefore, the objective of this study was to quantify the interaction effects of climate change, LULCC, and best management practices on the spatiotemporal dynamics of SOC-N pools and other ecosystem behaviors by devising a process-based model.

Materials and methods

Description of study region

Ardahan watershed with a land surface area of about 56 km^2 was selected as the study region and has a mean altitude of 2400 $\pm$ 400 m above sea level (Fig. 1). Based on the long-term data (1970–2000), the study region had a long-term mean annual temperature of 3.3 °C with a mean minimum and maximum temperature of − 9.9 °C in January and 14.8 °C in August and a total annual precipitation of 673 mm with its maximum and minimum fall from May to June and January to February, respectively (https://www.worldclim.org/data/worldclim21.html).

Based on a meteorological station installed in the study region, the six variables in Table 1 were also measured from 31 October 2018 to 19 September 2019. Its dominant soil type is haplic chernozems, with a mean slope of $13 \pm 11\%$. According to CORINE (2012), evergreen forests and grasslands are its dominant land covers.

Field sampling strategy

The entire study region was divided into the grids of 1 km^2. A systematic random sampling design with a minimum distance of 100 m between each sampling point was adopted to represent all the different ecosystem types using ArcGIS (Fig. 1). From the resultant 97 sampling points, soil samples for a depth of 0 to 30 cm were gathered in July 2018. The soil samples were oven-dried at 45 °C, grinded using ceramic and glass

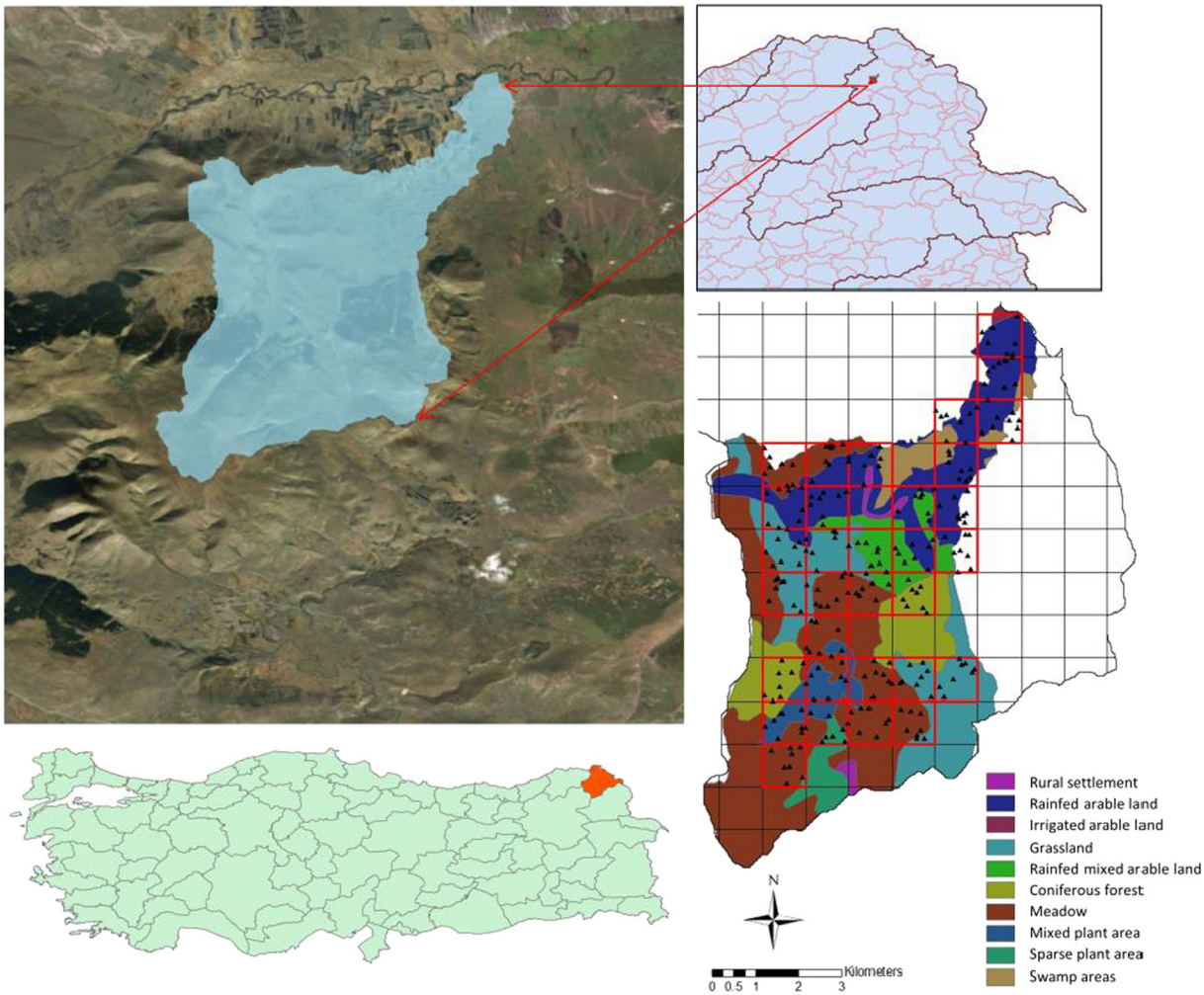

Fig. 1 Location map of Ardahan watershed and spatial distribution of soil sampling points and land uses/covers based on CORINE (2012) in the study region

mortars, sieved through a 2-mm sieve, and analyzed to determine the total C and N contents using a CHNS elemental analyzer (Thermo Scientific Flash 2000, Germany). These values were converted to the SOC-N stock values (t C or N/ha) in 2018 as follows (FAO 2019):

Table 1 Descriptive statistics of meteorological station data in the study region from 31 October 2018 to 19 September 2019

Climatic variable	Mean	SD	CV	Min	Median	Max	IQR
Temperature (°C)	9.5	8.3	86.9	−13.1	9.7	32.1	12.7
Relative humidity (%)	60.5	22.5	37.1	8.8	59.8	100.0	29.6
Wind direction (compass degree)	212.7	98.2	46.2	0.1	240.6	359.9	178.2
Wind speed (m/s)	1.7	1.2	69.3	0.0257	1.4	7.5	1.3
Net solar radiation (W/m^2)	311.4	223.8	71.9	0.02	278.2	857.4	371.7
Evapotranspiration (mm/day)	8.9	6.3	70.8	0.3	7.8	24.1	10.8

$$\mathrm{SOC\ (t\ C/ha)} = \mathrm{SOC\ content\ (g/kg)/1000} \times \mathrm{BD(kg/m^3)} \times (1-\mathrm{CF(\%)/100}) \times SD(\mathrm{m}) \times 10 \quad (1)$$

where *BD* and *CF* refer to bulk density and coarse fragment fraction, respectively, which were on average estimated at 1370 kg/m^3 and 12% based on the 97 soil samples. *SD* is the soil depth of 0.3 m used in this study.

In this study, the following remotely sensed data were used from the following sources: evapotranspiration (ET) (MOD16A2) (https://search.earthdata.nasa.gov/search?q=MOD16A2), land surface temperature (LST) (MOD11A2) (https://search.earthdata.nasa.gov/search?q=MOD11A2), and net primary productivity (NPP) (MOD17A3) (https://search.earthdata.nasa.gov/search?q= MOD17A3) from Moderate Resolution Imaging Spectroradiometer (MODIS), land-use dynamics (CORINE) (https://land.copernicus.eu/pan-european/corine-land-cover/clc-2012), precipitation (PPT) (https://www.worldclim.org/data/worldclim21.html), representative concentration pathways (RCP) 6.0 Community Climate System Model-4 (CCSM4) precipitation (https://www.worldclim.org/data/cmip6/cmip6_clim2.5m.html), GAI & ET0 Climate Database V2 (https://cgiarcsi.

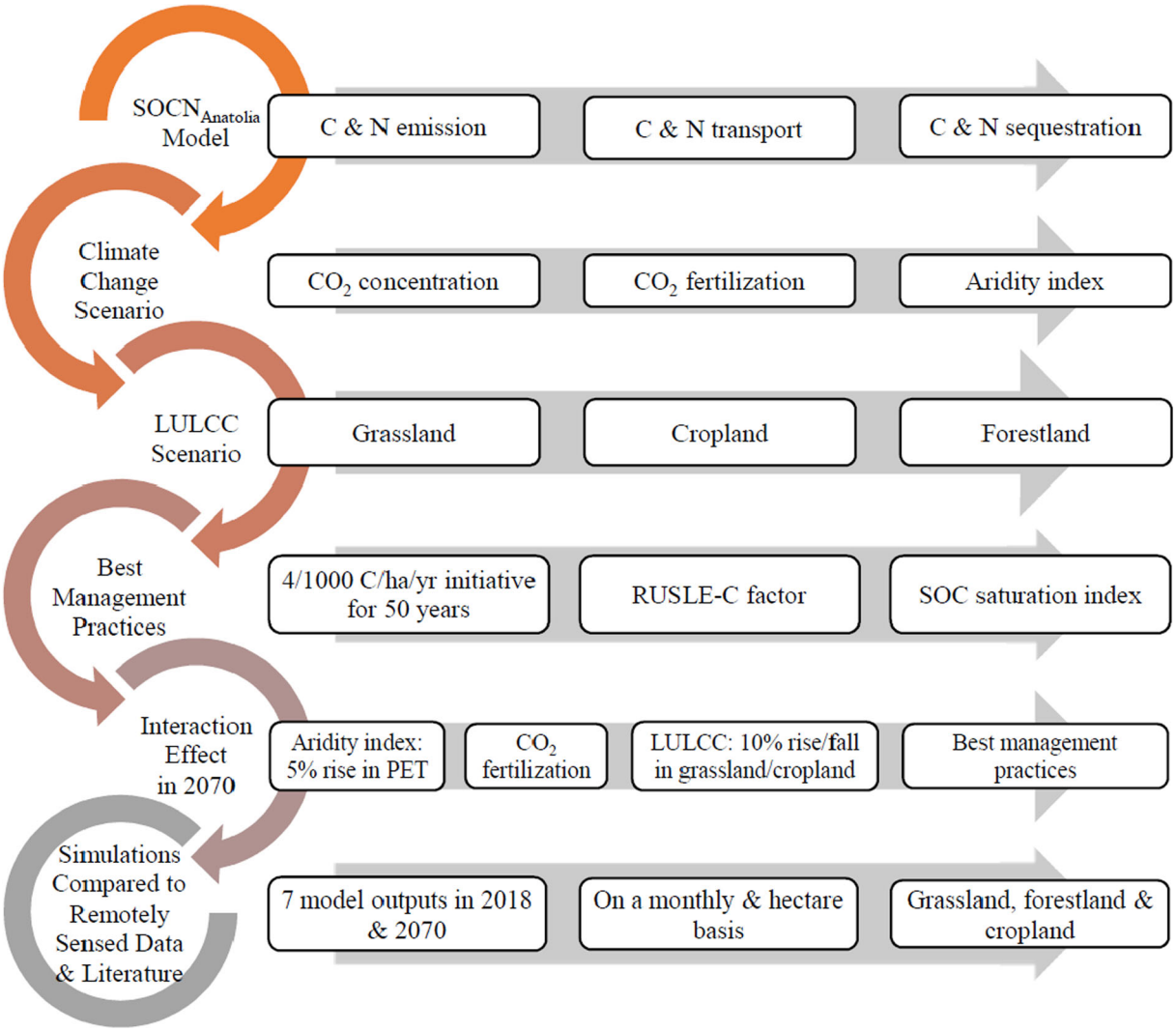

Fig. 2 A flowchart as an overview of the methodological steps and their sequential order adopted in this study

community/2019/01/24/global-aridity-index-and-potential-evapotranspiration-climate-database-v2/), and RUSLE-C factor.

Modeling process

The flowchart is illustrated as an overview of the separate steps and their sequential order adopted in this study in Fig. 2. Our model named SOC-$N_{Anatolia}$ was based on the algorithms of CENTURY (Parton et al. 1993), SOCRATES (Grace et al. 2006), and CEM (Evrendilek and Wali 2001). The model runs on a monthly basis at a 1-km^2 spatial resolution whose simulations are expressed in t C or N/ha/month and uses geographical information systems (GIS) and remotely sensed data. SOC-$N_{Anatolia}$ consisted of metabolic and structural litter and active, slow, and passive SOC-N pools (Fig. 3). The allocation ratio of 3, 37, and 60% was assumed to partition the total SOC-N stocks into active, slow, and passive ones, respectively (Parton et al. 1993; Evrendilek and Wali 2001). The model generates the following eight outputs of NPP, SOC-N pools, soil C:N ratio, soil respiration, total N emission, and sediment C-N transport effluxes for cropland, grassland, and forest. NPP flux was estimated using the temperature-dependent Miami model (Lieth 1975) as follows:

$$\mathrm{NPP}\left(\mathrm{g\ C/m^2/year}\right) = 3000/\left(1 + e^{1.315-0.0119*T}\right) \times 0.45 \quad (2)$$

where T refers to air temperature and *0.45* is the C content of the dry weight plant biomass. According to the allocation parameters used by the SOCRATES model (Grace et al. 2006), NPP was partitioned into the leaf, branch, stem, and root biomass parts as well as into labile (metabolic) and recalcitrant (structural) litter components depending on the ecosystem type. In order for the vegetation growing period to be determined, the threshold temperature of 5 °C was assumed for its start and end times (Evrendilek and Wali 2001). According to CENTURY (Parton et al. 1993), the maximum decomposition rates (k, $month^{-1}$) used in this study were 0.3625, 1.3875, 0.55416667, 0.0166667, and 0.000375 for the structural and metabolic litter and active, slow, and passive SOC-N pools, respectively (Fig. 3).

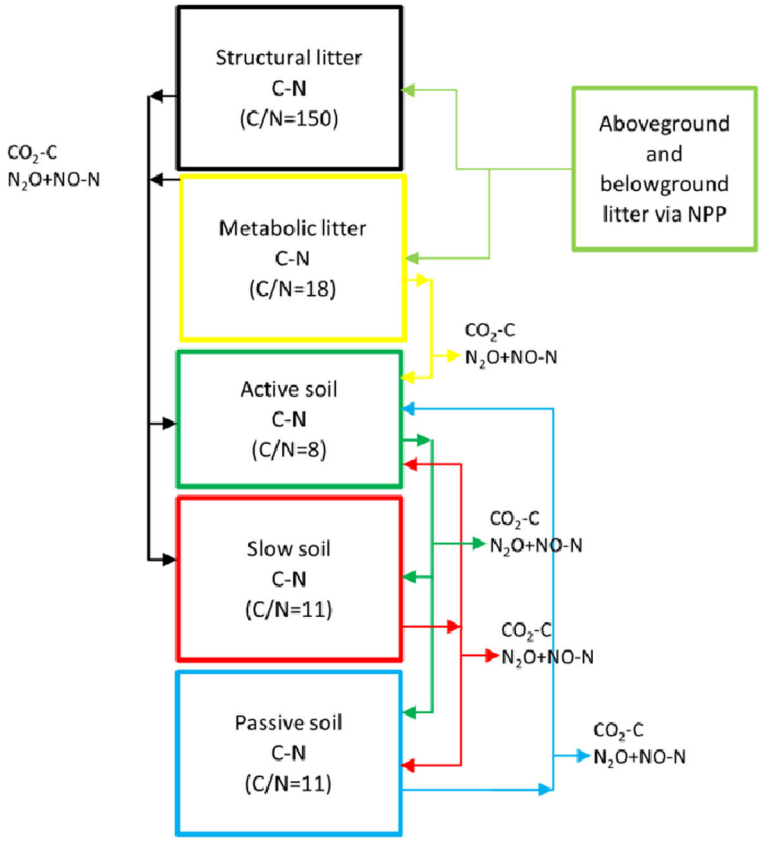

Fig. 3 Algorithm of SOC-$N_{Anatolia}$ model

Scenario analyses

Climate change

The main components of global climate change include air temperature rise, altered PPT and ET regimes, and increased atmospheric CO_2 concentration. In this study, an aridity index that reflected the composite change in temperature, ET, and PPT was developed for the period of 2018 to 2070 at a 1-km^2 spatial resolution thus:

$$\text{Aridity Index} = \frac{\text{PPT}}{\text{PET}} \quad (3)$$

where *PPT* is the precipitation (mm/month) and *PET* is the potential evapotranspiration (mm/month).

Monthly PPT data for 2070 (average of 2061–2080) were obtained from the RCP 6.0 scenario of CCPM4 composite climate model with IPPC5 (CMIP5) data scaled down at a resolution of 30 arc seconds (approximately 1 km) (https://www.worldclim.org/cmip5_30s). Monthly mean PET data for the period of 1970–2000 were obtained from Trabucco and Zomer (2019) (https://figshare.com/articles/Global_Aridity_Index_and_Potential_Evapotranspiration_ET0_Climate_Database_v2/7504448/3). Future PET data were created using the four scenarios of 5% and 15% increases and decreases by 2070. The aridity index was incorporated in the model as the regulatory factor, with its values below or above unity reducing and enhancing the SOC-N and NPP values, respectively.

The atmospheric CO_2 concentration ($AtmCO_2$) was assumed to rise in the model simulations from the current level of 400 to 670 ppmv in 2070 according to RCP 6.0 as an exponential function of time (Goudriaan 1992; Goudriaan and Zadoks 1995) thus:

Fig. 4 SOC-N saturation index map of the study area

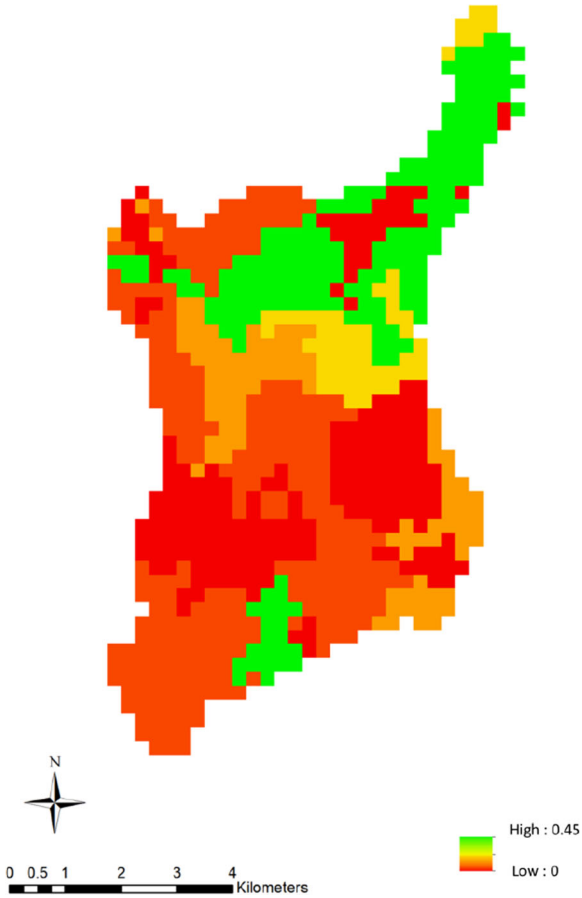

Fig. 5 RUSLE-C index map of the study area

$$\mathrm{AtmCO_2} = 400 \times (1 + (0.00084))^{t} \quad (4)$$

The CO_2 fertilization (CO_2-F) effect on NPP was expressed as a logarithmic function as follows (Kimball et al. 1993):

$$\mathrm{CO_2{-}F} = 1 + 0.6 \times \log(\mathrm{AtmCO_2})/400) \quad (5)$$

where *0.6* is the coefficient used for the vegetation response to CO_2-F.

Land-use and land-cover change

The following three scenarios were adopted to map LULCC of the study region for 2070: (1) 10% deforestation in return for 10% increase in croplands; (2) 10% decrease in croplands in return for 10% increase in grasslands; and (3) 10% decrease in grasslands in return for 5% increase in forestland and 5% increase in cropland. The future map of LULCC among cropland, forestland, and grassland in 2070 was created converting the 1-km^2 resolution grids of the current LULCC map in accord with the above three scenarios.

Best management practices

The 4/1000 C/ha/year initiative for 50 years according to COP21 (2015) was adopted to quantify the temporal effect of the best management practices on SOC-N stocks. This initiative was made to spatially change equally depending on the indices of SOC-N saturation and RUSLE-C (land-cover management) (2/1000 + 2/1000). The SOC-N saturation index (Fig. 4) ranged from 0 to 1, thus representing the peak and valley for the SOC-N saturation, respectively, and was factored in the initiative thus:

$$2/1000 \times \mathrm{SOC{-}N\ Saturation\ Index} \times 50\ \mathrm{yr} \quad (6)$$

The RUSLE-C index (Fig. 5) also varied between 0 and 1, thus indicating areas with low and high potential for improvement, respectively, and was incorporated in the initiative thus:

$$2/1000 \times \mathrm{RUSLE{-}C\ Index} \times 50\ \mathrm{yr} \quad (7)$$

Interaction effects

The four components whose interaction effects were simulated consisted of aridity index with 5% increase in PET, CO_2 fertilization, 10% decrease in croplands in return for 10% increase in grasslands, and the best management practices.

Results and discussion

The geo-referenced point values of the SOC-N stocks for a depth of 0–30 cm in 2018 were interpolated using the inverse distance weighting (IDW) approach. The IDW-based maps of the SOC-N stocks were used as the initial values to run SOC-$N_{Anatolia}$. The eight monthly model outputs included NPP, SOC-N stocks, soil C:N

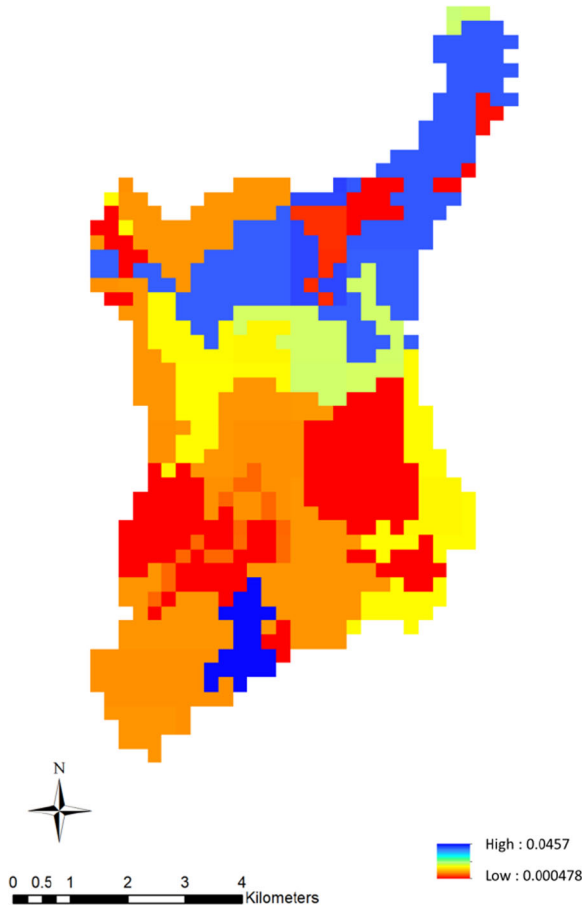

Fig. 6 Map of potential increase in SOC-N stock (t C/ha) for the next 50 years (in 2070) based on the adoption of the best management practices

ratio, soil respiration, total N (N_2O- and NO-N) emission, and sediment C-N transport effluxes.

Based on the combination of the 4/1000 initiative and the SOC-N saturation and RUSLE-C maps, the map in Fig. 6 was created to illustrate the spatial distribution of the potential increase in the SOC-N stocks in 2070 as a result of the adoption of the best management practices. According to the resultant map (Fig. 6), the blue and yellow colors indicated the first and second priority areas where the SOC-N pools can be maximized, respectively. The red color showed the areas where the SOC-N storage should be maintained.

The model outputs were compared to both related remote sensing data and related literature in order to test the model performance. The SOC-N field campaign results in 2018 were compared to SoilGrids data at the 250-m resolution (SoilGrids-250) (Fig. 7) for each ecosystem type in terms of means and standard deviations (Fig. 8). The maximum mean SOC pool belonged to the cropland and forestland, while the minimum one occurred with the forestland and grassland according to the SoilGrids-250 and in situ field datasets, respectively (Fig. 8). Also, the SoilGrids-250 data exhibited a higher variability than did the field data for each ecosystem type (Fig. 8). The mean SOC pool of our ground truth soil data was 16 and 18% lower for the cropland (62.6 ± 5.2 t C/ha) and the grassland (59.8 ± 3.9 t C/ha), respectively, and 4% higher for the forest (66.3 ± 2.6 t C/ha) than that of the SoilGrids-250 data (Table 2). In other words, the SoilGrids-250 data underestimated the forest SOC pool but overestimated the cropland and grassland SOC pools in the high altitude ecosystems of the Ardahan watershed. The SoilGrids-250 data overestimated the in situ SON storage by 17.5 and 13% for the forest and cropland, respectively, and underestimated it by 142% for the grassland (Table 2). Shirato (2017) reported that the average SOC content (31 g C/kg) of the SoilGrids-250 data for the agricultural land of Rwanda was about 25% higher than the in situ field data of 800 soil samples (25 g C/kg) ($r^2 = 0.05$).

The SOC-N stocks and their C/N ratios in 2018 and 2070 are illustrated in Fig. 9, while the remaining model outputs in 2018 and 2070 are presented in Tables 2 and 3, respectively. The global values from the related literature and the local values of the remotely sensed data were compared to our model outputs for 2018 (Table 2). The difference between the model predictions and the remotely sensed data for the study region ranged from −64% for the cropland NPP to 142% for the grassland SOC pool (the negative and positive signs denote the model underestimation and overestimation, respectively) (Table 2). The difference between the model

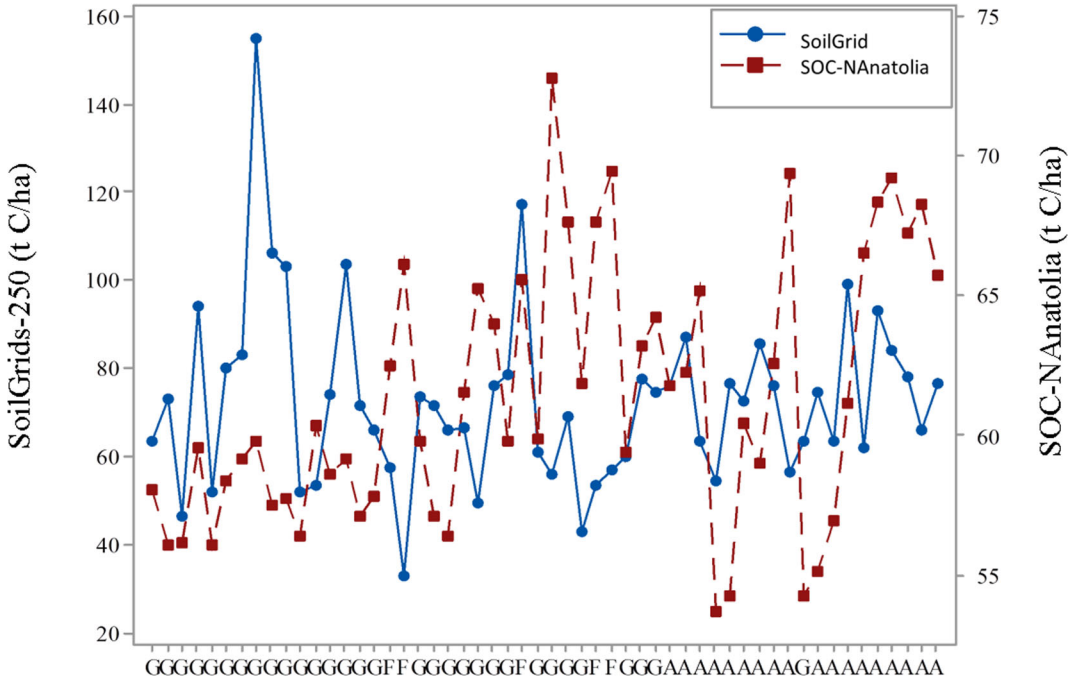

Fig. 7 A comparison of SoilGrids-250 data versus field data for SOC stocks in 2018 for each land cover (G, grassland; F, forestland; and A, agricultural land) used to run $SOC\text{-}N_{Anatolia}$

predictions for the study region and the global mean values based on the related literature varied between −97% for the sediment C and N effluxes from the LULCC and 60% for the total N emission from the grassland (Table 2).

The MOD17A3H V006 product at a 500-m resolution for the study region showed that the modeled NPP was lower than the MODIS NPP by the range of 23% for the forest to 64% for the cropland on a monthly basis (Table 2). The related literature indicated that our monthly model predictions were lower than the global mean soil respirations of forest, grassland, and cropland (Raich and Tufekcioglu 2000) by 77, 93, and 95%, respectively (Table 2). The cold continental climate, the high altitude, and the short vegetation period of the study region appeared to account for the lower NPP and soil respiration values than the global mean values for the ecosystem types (Koven et al. 2017). The monthly model predictions of the total N emission were lower by 88 and 22% for the forest and cropland, respectively, and higher

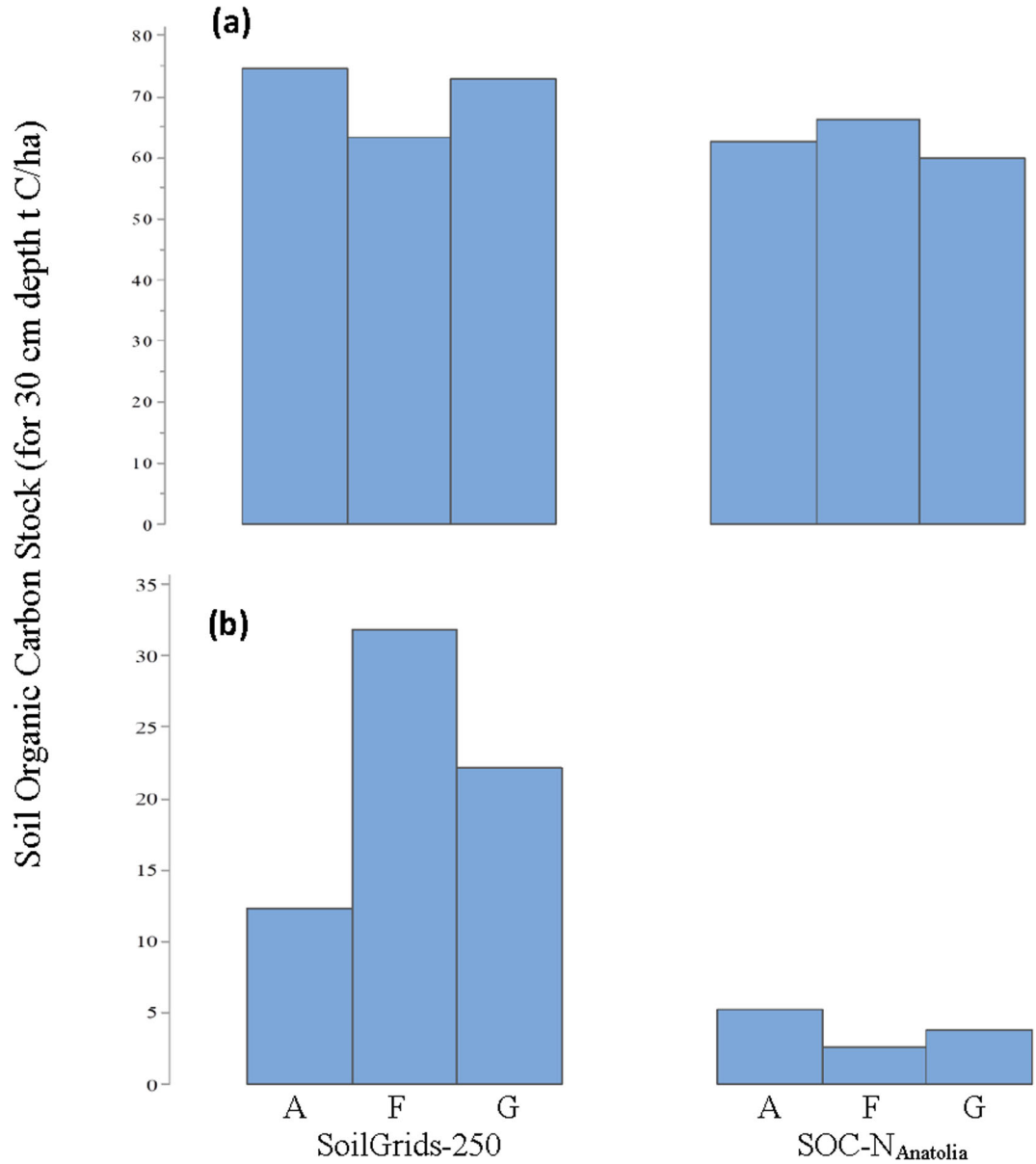

Fig. 8 A comparison of SoilGrids-250 data versus field data in terms of **a** mean and **b** standard deviation values of SOC-N stock for each land-cover class (A, arable land; F, forest; and G, grassland)

Table 2 A comparison of the seven SOC-$N_{Anatolia}$ model outputs for 2018 versus related literature

Model output	Unit	Forest	Reference value	Grassland	Reference value	Cropland	Reference value
Monthly NPP	t C/ha/month						
mean ± SD (% change) min-max		1.03 ± 0.22 (− 23) 0.59–1.50	1.33 ± 0.08 6.31–7.39 (MOD17A3H)	0.60 ± 0.08 (− 50) 0.44–1.50	1.20 ± 0.08 5.46–6.41 (MOD17A3H)	0.48 ± 0.10 (− 64) 0.44–1.30	1.23 ± 0.08 5.57–6.69 (MOD17A3H)
SOC stock	t C/ha/year						
mean ± SD (% change) min-max		66.3 ± 2.6 (4.5) 62.5–69.4	63.3 ± 31.8 32.4–117.2 (SoilGrids-250)	59.8 ± 3.9 (− 18) 54.2–72.8	72.9 ± 22.2 42.8–155.1 (SoilGrids-250)	62.6 ± 5.2 (− 16) 53.7–69.4	74.6 ± 12.3 54.1–98.8 (SoilGrids-250)
SON stock	t N/ha/year						
mean ± SD (% change) min-max		5.23 ± 0.14 (− 17.5) 4.89–5.64	6.36 ± 0.21 5.66–6.87 (SoilGrids-250)	5.15 ± 0.27 (142) 4.62–6.34	2.13 ± 0.57 0.20–6.80 (SoilGrids-250)	5.56 ± 0.35 (− 13) 4.68–6.12	6.37 ± 0.37 5.42–6.94 (SoilGrids-250)
Soil respiration	t C/ha/month						
mean ± SD (% change) min-max		0.03 ± 0.001 (− 77) 0.02–0.04	0.13 ± 0.01 0.32–0.61 (Raich and Tufekcioglu 2000)	0.024 ± 0.01 (− 93) 0.021–0.036	0.34 ± 0.03 (Raich and Tufekcioglu 2000)	0.024 ± 0.001 (− 95) 0.021–0.035	0.52 ± 0.04 (Raich and Tufekcioglu 2000)
Total N emission ($N_2O + NO$)	t N/ha/month						
mean ± SD (% change) min-max		$2.6 \times 10^{-4} \pm 1 \times 10^{-5}$ (− 88) 2.2×10^{-4}–2.9×10^{-4}	$2.2 \times 10^{-3} \pm 2.1 \times 10^{-3}$ (Stehfest 2005)	$2.4 \times 10^{-4} \pm 1 \times 10^{-5}$ (60) 2.2×10^{-4}–2.9×10^{-4}	$1.5 \times 10^{-4} \pm 3 \times 10^{-5}$ 1×10^{-4}–2×10^{-4} (Stehfest 2005)	$2.5 \times 10^{-4} \pm 9 \times 10^{-5}$ (− 22) 2.3×10^{-4}–2.8×10^{-4}	$3.2 \times 10^{-4} \pm 9 \times 10^{-5}$ 1.9×10^{-4}–4.4×10^{-4} (Stehfest 2005)
Sediment C efflux	t C/ha/month						
mean ± SD (% change) min-max		$2.7 \times 10^{-4} \pm 7 \times 10^{-5}$ (− 97) 2.5×10^{-4}–2.9×10^{-4}	$9 \times 10^{-3} \pm 1.7 \times 10^{-2}$ 3.5×10^{-5}–1.07×10^{-1} (Vanmaercke et al. 2011)	$2.7 \times 10^{-4} \pm 1 \times 10^{-5}$ (− 97) 2.4×10^{-4}–3.2×10^{-4}	$9 \times 10^{-2} \pm 1.7 \times 10^{-2}$ 3.5×10^{-5}–0.107 (Vanmaercke et al. 2011)	$2.8 \times 10^{-4} \pm 1 \times 10^{-5}$ (− 97) 2.4×10^{-4}–3.1×10^{-4}	$9.15 \times 10^{-3} \pm 1.7 \times 10^{-2}$ 3.5×10^{-5}–0.107 (Vanmaercke et al. 2011)
Sediment N efflux	t N/ha/month						
mean ± SD (% change) min-max		$2.6 \times 10^{-4} \pm 1 \times 10^{-4}$ (− 71) 2.2×10^{-4}–2.9×10^{-4}	$9 \times 10^{-4} \pm 1.7 \times 10^{-3}$ 4×10^{-6}–1.07×10^{-2} (Vanmaercke et al. 2011)	$2.4 \times 10^{-5} \pm 1 \times 10^{-6}$ (− 97) 2.1×10^{-5}–2.9×10^{-5}	$9 \times 10^{-4} \pm 1.7 \times 10^{-2}$ 4×10^{-6}–1.07×10^{-2} (Vanmaercke et al. 2011)	$2.5 \times 10^{-5} \pm 1 \times 10^{-6}$ (− 97) 2.1×10^{-5}–2.8×10^{-5}	$9 \times 10^{-4} \pm 1.7 \times 10^{-3}$ 4×10^{-6}–1.07×10^{-2} (Vanmaercke et al. 2011)

by 60% for the grassland than the global mean values (Stehfest 2005) (Table 2). All the predicted monthly sediment C and N effluxes were lower 97% than the global mean values (Vanmaercke et al. 2011), regardless of the ecosystem type, except for the sediment N efflux from the forest being 71% lower (Table 2).

The simulated interaction among the four components (aridity index with the 5% increase in PET, CO_2 fertilization, the 10% fall in croplands in exchange for the 10% rise in grasslands, and the best management practices) yielded the spatial distribution maps of the eight monthly model outputs between 2018 and 2070 (a total of 52 years × 12 months × 8 outputs = 4992 maps). The simulated interaction effect in 2070 resulted in the three minimum increases in the annual SON stock by 3.8 and 5.2% for the forest and grassland, respectively, and the monthly sediment N flux for the grassland by 4.2% (Table 3). The interaction led to the three maximum increases in the monthly sediment C effluxes from the cropland, grassland, and forest by 139.3, 137.1, and 133.3%, respectively.

The three interaction-induced minimum decreases were the monthly grassland and cropland NPP by − 14.6 and − 35.4%, respectively, and the monthly total N

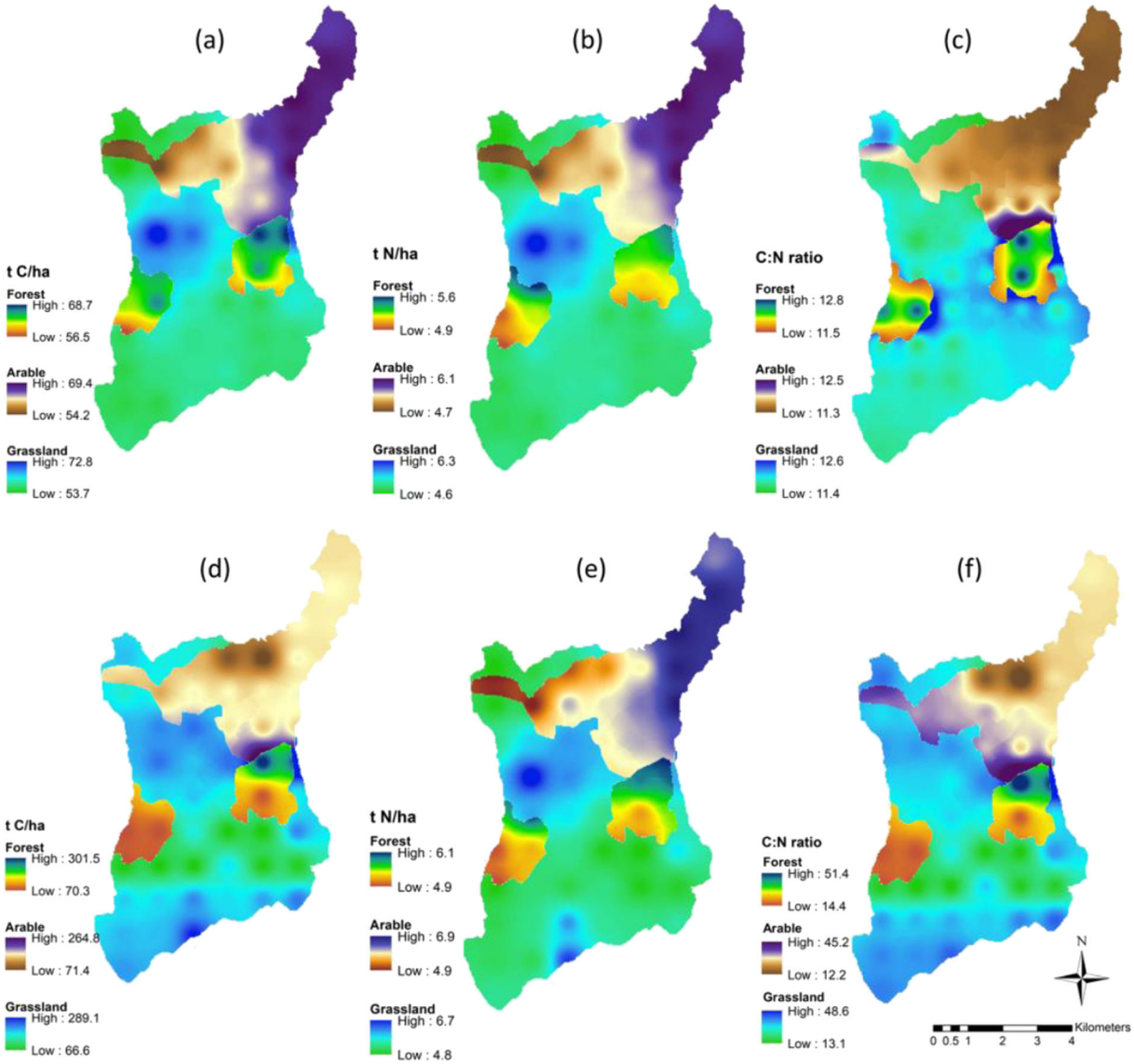

Fig. 9 Spatial distribution maps of **a** SOC and **b** SON stocks and **c** C/N ratio in 2018 and **d**–**f** 2070 in response to the interaction effect scenario simulated using SOC-$N_{Anatolia}$

Table 3 SOC-$N_{Anatolia}$ predictions of the interaction effects on each land cover in 2070 relative to the initial conditions in 2018 in terms of the seven model outputs

	Unit	Forest	Grassland	Cropland
Monthly NPP	t C/ha/month			
mean ± SD (% change) min-max		0.63 ± 0.13 (31.25) 0.35–0.93	0.41 ± 0.06 (−14.6) 0.29–0.89	0.31 ± 0.05 (−35.4) 0.27–0.77
SOC stock	t C/ha/year			
mean ± SD (% change) min-max		136.28 ± 55.17 (114.2) 70.33–301.51	137.44 ± 28.79 (129.7) 66.57–289.08	144.56 ± 20.68 (127.1) 71.38–264.77
SON stock	t N/ha/year			
mean ± SD (% change) min-max		5.43 ± 0.27 (3.8) 4.89–6.06	5.43 ± 0.35 (5.4) 4.84–6.74	6.09 ± 0.47 (9.5) 4.93–6.87
Soil respiration	t C/ha/month			
mean ± SD (% change) min-max		$5.9 \times 10^{-3} \pm 3 \times 10^{-3}$ (− 80.3) 2×10^{-3}–1.5×10^{-3}	0.0064 ± 0.002 (− 73.3) 1.6×10^{-3}–1.5×10^{-2}	0.0066 ± 0.001 (72.5) 1.9×10^{-3}–1.3×10^{-3}
N emission ($N_2O + NO$)	t N/ha/month			
mean ± SD (% change) min-max		$4.5 \times 10^{-5} \pm 3 \times 10^{-5}$ (− 82.7) 4×10^{-6}–1.2×10^{-4}	$6 \times 10^{-5} \pm 3 \times 10^{-5}$ (− 75.0) 4×10^{-6}–2.3×10^{-4}	$1.1 \times 10^{-4} \pm 3 \times 10^{-5}$ (− 56.0) 6×10^{-6}–1.6×10^{-4}
Sediment C efflux	t C/ha/month			
mean ± SD (% change) min-max		$6.3 \times 10^{-5} \pm 3 \times 10^{-4}$ (133.3) 3.3×10^{-4}–1.4×10^{-3}	$6.4 \times 10^{-4} \pm 1 \times 10^{-4}$ (137.1) 3.1×10^{-4}–1.3×10^{-3}	$6.7 \times 10^{-4} \pm 1 \times 10^{-4}$ (139.3) 3.3×10^{-4}–1.2×10^{-3}
Sediment N efflux	t N/ha/month			
mean ± SD (% change) min-max		$2.5 \times 10^{-5} \pm 1 \times 10^{-6}$ (− 90.5) 2.3×10^{-5}–2.8×10^{-5}	$2.5 \times 10^{-5} \pm 1.6 \times 10^{-6}$ (4.2) 2.3×10^{-5}–3.1×10^{-5}	$2.8 \times 10^{-5} \pm 2 \times 10^{-6}$ (12.0) 2.3×10^{-5}–3.2×10^{-5}

($N_2O + NO$) emission from the cropland by − 56.0%. The interaction exerted the greatest negative impact on the monthly sediment N efflux, total N emission, and soil respiration from the forest by − 90.5, − 82.7, and − 80.3%, respectively (Table 3). By 2070, the monthly NPP increased for the forest but decreased for the grassland and cropland, whereas the monthly sediment N efflux exhibited the opposite pattern (Table 3). The monthly soil respiration decreased for the forest and grassland but increased for the cropland. Regardless of the ecosystem type, the increasing trends occurred with the monthly sediment C efflux and the annual SOC-N storage, whereas the decreasing trend was observed only with the monthly total N emission (Table 3).

The soil C:N ratio varied between 11.3 in the cropland and 12.8 in the forest in 2018 but significantly rose between 12.2 in the cropland and 51.4 in the forest in response to the interaction effect (Fig. 9). The high soil C:N ratios were previously reported to typically underlay forests, peatlands, and wetlands in northern, high altitude, and/or precipitation-intense ecosystems (Helliwell et al. 2001; Watt and Palmer 2012; Ballabio et al. 2019). The high soil C:N ratios were considered to be conducive to greater immobilization and denitrification rates of N as well as indicative of low soil fertility (Helliwell et al. 2001; Watt and Palmer 2012; Ballabio et al. 2019). The extremely low mean annual temperature of the study region appeared to be the primary driver of the high C:N ratios projected in 2070.

Conclusions

The SOC-$N_{Anatolia}$ model integrated both temporal and spatial dynamics on a monthly and hectare bases. Its simulations for the 52-year period (2018–2070) predicted the interaction effects of the four human-induced drivers of climate change (CO_2 fertilization and increased aridity), land-use change, and the best management practices on the three high altitude ecosystem types. The best management practices were turned into a spatiotemporal composite index by introducing the SOC-N stock saturation concept and combining it with the RUSLE-C factor map and the 4/1000 initiative. In general, the model successfully predicted the

eight variables according to the global mean values from the related literature and the local values of the remotely sensed data although the literature-derived generic model parameters were not calibrated using the ground observation values. Not only can SOC-$N_{Anatolia}$ help to better understand the emergent ecosystem behaviors generated by the interaction among drivers, pressures, states, impacts, and responses in a changing climate, land use, and land management but also can provide practical and dynamic insights into where to best intervene in the ecosystem structure and function. Its simulation capability of sediment C-N transport effluxes enables its outputs to be coupled to the quantification of the metabolism dynamics of the aquatic ecosystems by the other GIS-based watershed modeling tools such as MapShed, MOHID Land, and SWAT. It also plays a significant role in bridging the gaps between the remotely sensed data and the understanding of emergent ecosystem behaviors in terms of the fine versus coarse resolutions of the spatiotemporal datasets and the formulation and implementation of public policy actions. In order for the reliable and robust decisions to be ensured, further validations remain to be conducted so as to operate the model in ecosystems where diverse terrain types and climate features are dominant.

Acknowledgments We thank Haluk Fidan and Ceren Bozkurt for their help with the analysis of soil samples in laboratory.

Authors' contributions This article is extracted from Kadir Yildiz's MSc thesis. Nusret Karakaya and Fatih Evrendilek were co-supervisors for his MSc thesis and responsible for conceptualization, securing the TUBITAK funding, and drafting the article. Seref Kilic was responsible for soil sampling, analysis and mapping.

Funding information This research was funded by the Turkish Scientific and Technological Research Council (TUBITAK) under the Grant number: 117Y193.

Compliance with ethical standards

Conflict of interest The authors declare that they have no conflict of interest.

Ethics approval Not applicable.

Consent Not applicable.

References

Ballabio, C., Lugato, E., Fernández-Ugalde, O., Orgiazzi, A., Jones, A., Borrelli, P., Montanarella, L., & Panagos, P. (2019). Mapping LUCAS topsoil chemical properties at European scale using Gaussian process regression. *Geoderma, 355*, 113912. https://doi.org/10.1016/j.geoderma.2019.113912.

Churkina, G., Zaehle, S., Hughes, J., Viovy, N., Chen, Y., Jung, M., Heumann, B. W., Ramankutty, N., Heimann, M., & Jones, C. (2010). Interactions between nitrogen deposition, land cover conversion, and climate change determine the contemporary carbon balance of Europe. *Biogeosciences, 7*(9), 2749–2764. https://doi.org/10.5194/bg-7-2749-2010.

Elmendorf, S. C., Henry, G. H. R., Hollister, R. D., Björk, R. G., Bjorkman, A. D., Callaghan, T. V., Collier, L. S., Cooper, E. J., Cornelissen, J. H. C., Day, T. A., Fosaa, A. M., Gould, W. A., Grétarsdóttir, J., Harte, J., Hermanutz, L., Hik, D. S., Hofgaard, A., Jarrad, F., Jónsdóttir, I. S., Keuper, F., Klanderud, K., Klein, J. A., Koh, S., Kudo, G., Lang, S. I., Loewen, V., May, J. L., Mercado, J., Michelsen, A., Molau, U., Myers-Smith, I. H., Oberbauer, S. F., Pieper, S., Post, E., Rixen, C., Robinson, C. H., Schmidt, N. M., Shaver, G. R., Stenström, A., Tolvanen, A., Totland, Ø., Troxler, T., Wahren, C. H., Webber, P. J., Welker, J. M., & Wookey, P. A. (2012). Global assessment of experimental climate warming on tundra vegetation: Heterogeneity over space and time. *Ecology Letters, 15*, 164–175. https://doi.org/10.1111/j.1461-0248.2011.01716.x.

Ernakovich, J. G., Hopping, K. A., Berdanier, A. B., Simpson, R. T., Kachergis, E. J., Steltzer, H., & Wallenstein, M. D. (2014). Predicted responses of arctic and alpine ecosystems to altered seasonality under climate change. *Global Change Biology, 20*, 3256–3269. https://doi.org/10.1111/gcb.12568.

Evrendilek, F., & Wali, M. K. (2001). Modelling long-term C dynamics in croplands in the context of climate change: A case study from Ohio. *Environmental Modelling & Software, 16*(4), 361–375. https://doi.org/10.1016/S1364-8152(00)00089-X.

Goudriaan, J. (1992). Biosphere structure, carbon sequestering potential and the atmospheric ^{14}C carbon record. *Journal of Experimental Botany, 43*, 1111–1119. https://doi.org/10.1093/jxb/43.8.1111.

Goudriaan, J., & Zadoks, J. C. (1995). Global climate change: Modelling the potential responses of agro-ecosystems with special reference to crop protection. *Environmental Pollution, 87*, 215–224. https://doi.org/10.1016/0269-7491(94)P2609-D.

Grace, P. R., Ladd, J. N., Robertson, G. P., & Gage, S. H. (2006). SOCRATES—A simple model for predicting long-term changes in soil organic carbon in terrestrial ecosystems. *Soil Biology & Biochemistry, 38*, 1172–1176. https://doi.org/10.1016/j.soilbio.2005.09.013.

He, X., Liang, J., Zeng, Y., & Li, X. (2019). The effects of interaction between climate change and land-use/ cover change on biodiversity-related ecosystems services. *Global Challenges*, 1800095. https://doi.org/10.1002/gch2.201800095,

Helliwell, R. C., Ferrier, R. C., & Kernan, M. R. (2001). Interaction of nitrogen deposition and land use on soil and water quality in Scotland: Issues of spatial variability and scale. *Science of the Total Environment, 265*, 51–63. https://doi.org/10.1016/S0048-9697(00)00649-5.

Kimball, B. A., Mauney, J. R., Nakayama, F. S., Idso, S. B. (1993). Effects of increasing atmospheric CO on vegetation. In J. Rozema, H. Lambers, S. C. Van de Geijn, M. L. Cambridge (Eds.), *CO and biosphere. Advances in vegetation science*, vol 14. Dordrecht: Springer.

Koven, C. D., Hugelius, G., Lawrence, D. M., & Wieder, W. R. (2017). Higher climatological temperature sensitivity of soil carbon in cold than warm climates. *Nature Climate Change, 7*, 817–822. https://doi.org/10.1038/nclimate3421.

Lieth, H. (1975). Modelling the primary productivity of the world. In H. Lieth & R. H. Whittaker (Eds.), *Primary productivity of the biosphere* (pp. 237–263). New York: Springer-Verlag.

O'Rourke, S. M., Angers, D. A., Holden, N. M., & McBratney, A. B. (2015). Soil organic carbon across scales. *Global Change Biology, 21*, 3561–3574. https://doi.org/10.1111/gcb.12959.

Parton, W. J., Scurlock, J. M. O., Ojima, D. S., Gilmanov, T. G., Scholes, R. J., Schimel, D. S., Kirchner, T., Menaut, J. C., Seastedt, T., Garcia Moya, E., Kamnalrut, A., & Kinyamario, J. I. (1993). Observations and modeling of biomass and soil organic matter dynamics for the grassland biome worldwide. *Global Biogeochemical Cycles, 7*, 785–809. https://doi.org/10.1029/93GB02042.

Peters, M. K., Hemp, A., Appelhans, T., Becker, J. N., Behler, C., Classen, A., Detsch, F., Ensslin, A., Ferger, S. W., Frederiksen, S. B., Gebert, F., Gerschlauer, F., Gütlein, A., Helbig-Bonitz, M., Hemp, C., Kindeketa, W. J., Kühnel, A., Mayr, A. V., Mwangomo, E., Ngereza, C., Njovu, H. K., Otte, I., Pabst, H., Renner, M., Röder, J., Rutten, G., Schellenberger Costa, D., Sierra-Cornejo, N., Vollstädt, M. G. R., Dulle, H. I., Eardley, C. D., Howell, K. M., Keller, A., Peters, R. S., Ssymank, A., Kakengi, V., Zhang, J., Bogner, C., Böhning-Gaese, K., Brandl, R., Hertel, D., Huwe, B., Kiese, R., Kleyer, M., Kuzyakov, Y., Nauss, T., Schleuning, M., Tschapka, M., Fischer, M., & Steffan-Dewenter, I. (2019). Climate–land-use interactions shape tropical mountain biodiversity and ecosystem functions. *Nature, 568*, 88–92. https://doi.org/10.1038/s41586-019-1048-z.

Piao, S., Wang, X., Wang, K., Li, X., Bastos, A., Canadell, J. G., Ciais, P., Friedlingstein, P., & Sitch, S. (2020). Interannual variation of terrestrial carbon cycle: Issues and perspectives. *Global Change Biology, 26*(1), 300–318. https://doi.org/10.1111/gcb.14884.

Raich, J. W., & Tufekcioglu, A. (2000). Vegetation and soil respiration: Correlations and controls. *Biogeochemistry, 48*, 71–90. https://doi.org/10.1023/A:1006112000616.

Shirato, Y. (2017). Calculating changes in soil organic carbon in Japanese agricultural land by IPCC-tier 3 modeling approach: Use of modified Rothamsted carbon model. In proceedings of the global symposium on soil organic carbon (pp. 177).

Stehfest, E. (2005). Modelling of global crop production and resulting N_2O emissions. Dissertation, Universitaet Kassel, Kassel, Germany.

Stehfest, E., van Zeist, W., Valin, H., Havlik, P., Popp, A., Kyle, P., et al. (2019). Key determinants of global land-use projections. *Nature Communications, 10*, 2166. https://doi.org/10.1038/s41467-019-09945-w.

Trabucco, A., & Zomer, R. (2019). Global aridity index and potential evapotranspiration (ET_0) climate database v2. Figshare. Dataset: https://figshare.com/articles/Global_Aridity_Index_and_Potential_Evapotranspiration_ET0_Climate_Database_v2/7504448/3

Vanmaercke, M., Poesen, J., Verstraeten, G., de Vente, J., & Ocakoglu, F. (2011). Sediment yield in Europe: Spatial patterns and scale dependency. *Geomorphology, 130*(3–4), 142–161. https://doi.org/10.1016/j.geomorph.2011.03.010.

Watt, M. S., & Palmer, D. J. (2012). Use of regression kriging to develop a carbon: Nitrogen ratio surface for New Zealand. *Geoderma, 183*, 49–57. https://doi.org/10.1016/j.geoderma.2012.03.013.

Xiong, X., Grunwald, S., Myers, D. B., Ross, C. W., Harris, W. G., & Comerford, N. B. (2014). Interaction effects of climate and land use/land cover change on soil organic carbon sequestration. *Science of the Total Environment, 493*, 974–982. https://doi.org/10.1016/j.scitotenv.2014.06.088.

Yin, R., Eisenhauer, N., Schmidt, A., Gruss, I., Purahong, W., Siebert, J., & Schädler, M. (2019). Climate change does not alter land-use effects on soil fauna communities. *Applied Soil Ecology, 140*, 1–10. https://doi.org/10.1016/j.apsoil.2019.03.026.